Vibronic coupling and excited-state reaction dynamics of pyrazine in 11B2u(1ππ*) state by resonance Raman spectroscopy and CASSCF calculation

ARTICLE *in* JOURNAL OF RAMAN SPECTROSCOPY · OCTOBER 2012

Impact Factor: 2.67 · DOI: 10.1002/jrs.4074

11 AUTHORS, INCLUDING:

Xuming Zheng
Zhejiang Sci-Tech University
109 PUBLICATIONS **1,260** CITATIONS
SEE PROFILE

Wei-Hai Fang
Beijing Normal University
233 PUBLICATIONS **4,481** CITATIONS
SEE PROFILE

Research article

Journal of RAMAN SPECTROSCOPY

Received: 14 November 2011 Revised: 10 February 2012 Accepted: 2 March 2012 Published online in Wiley Online Library: 23 June 2012

(wileyonlinelibrary.com) DOI 10.1002/jrs.4074

Vibronic coupling and excited-state reaction dynamics of pyrazine in 1 $^1B_{2u}$ ($^1\pi\pi^*$) state by resonance Raman spectroscopy and CASSCF calculation

Jian-Li Guo,[a] Chong Liu,[a] Bin-Bin Xie,[a] Yan-Ying Zhao,[a] Ke-Mei Pei,[a] Hui-Gang Wang,[a] Xuming Zheng,[a]* Yue-Jie Ai,[b] Xue-Bo Chen,[b] Wei-Hai Fang[b]* and Chi Shun Yeung[c]

The photophysics and photochemistry of pyrazine ($C_4H_4N_2$, D_{2h}) after excitation to the S_2 (1 $^1B_{2u}$, $^1\pi\pi^*$) electronic state were studied by using the resonance Raman spectroscopy and complete active space self-consistent field method calculations. The B-band resonance Raman spectra in cyclohexane solvent were obtained at 266.0, 252.7, and 245.9 nm excitation wavelengths to probe the structural dynamics of pyrazine in the S_2 (1 $^1B_{2u}$, $^1\pi\pi^*$) state. Three electronic states 1 $^1B_{3u}$, 1 $^1B_{1g}$, and 1 $^1B_{2g}$ were found to couple with the S_2 (1 $^1B_{2u}$, $^1\pi\pi^*$) state. Two conical intersection (CI) points CI[$S_2(B_{2u})/S_1(B_{3u})$] and CI[S_1/S_0] and one transition state of the isomerization between pyrazine and pyrimidine were predicted to play important roles in the photochemistry of pyrazine. On the basis of the calculations, the mechanism of the photoisomerization reaction between pyrazine and pyrimidine has been proposed. Copyright © 2012 John Wiley & Sons, Ltd.

Supporting information may be found in the online version of this article.

Keywords: vibronic coupling; conical intersection; excited-state structural dynamics; resonance Raman; CASSCF computation

Introduction

Internal conversion or intersystem crossing through a conical intersection (CI) is the primary process underlying a number of ultrafast and selective photochemical processes in molecular systems.[1–4] The photophysics of pyrazine ($C_4H_4N_2$, D_{2h}) after excitation to the S_2 (1 $^1B_{2u}$, $^1\pi\pi^*$) electronic state has been studied experimentally and theoretically because of its significance in understanding the role of the CI in the ultrafast deactivation processes from upper excited states to lower ones. A low-lying CI between $S_2(^1B_{2u}, \pi\pi^*)$ and $S_1(^1B_{3u}, n\pi^*)$ was identified for pyrazine by semi-empirical calculations[5] and *ab initio* calculations.[6,7] It has been predicted that the out-of-plane vibrational mode Q_{10a} (b_{1g}) is the unique key vibrational mode that induces the vibronic coupling between S_2 and S_1, whereas the totally symmetric (a_g) normal modes of Q_1, Q_{6a}, and Q_{9a} are the primary tuning modes in the multidimensional potential energy surfaces (PESs).[6,7] Femtosecond time-resolved photoelectron spectroscopy experiments were used to study the ultrafast internal conversion from S_2 to S_1 of pyrazine through CI.[8–10] A recent femtosecond pump–probe photoelectron imaging spectroscopic study measured a 22 fs lifetime for the S_2 state of pyrazine and deuterated pyrazine,[10] which indicates that the underlying nonadiabatic electronic transition through a CI is extremely fast.

It has been known that irradiation of pyrazine at 253.7 nm undergoes the interchange of adjacent ring atoms that leads to the formation of pyrimidine,[11–14] whereas irradiation of pyrazine at 313.0 nm appears to induce almost no reaction to take place.[15,16] It was observed that irradiation of 2-methylpyrazine in the vapor phase leads to a mixture of 2-, 4-, and 5-methylpyrimidines. Similar photochemical valence isomerization can also be found in the dimethylpyrazine system. Complete active space self-consistent field (CASSCF) (6,6)/6-311G(d) and MP2-CASSCF level of theory computations revealed several reaction pathways for the photochemical transformations of methyl-substituted pyrazines in its first $^1\pi\pi^*$ excited state.[17] These results suggest that the photoisomerization of pyrazine is initiated in the $S_2(^1B_{2u}, \pi\pi^*)$ excited state of pyrazine and is completed on the ground-state PES of pyrimidine after passage through a CI between the PESs of pyrazine and pyrimidine, which appears to be consistent with the available experimental observations of the pyrimidine derivatives.

* *Correspondence to: Xuming Zheng, Department of Chemistry and State Key Laboratory of ATMMT(MOE), Zhejiang Sci-Tech University, Hangzhou, China 310018. E-mail: zhengxuming126@126.com*
Wei-Hai Fang, Department of Chemistry, Beijing Normal University, Beijing, China. E-mail: fangwh@bnu.edu.cn

a *Department of Chemistry and State Key Laboratory of ATMMT(MOE), Zhejiang Sci-Tech University, Hangzhou, China, 310018*

b *Department of Chemistry, Beijing Normal University, Beijing, China*

c *Department of Chemistry, The University of Hong Kong, Pokfulam Road Hong Kong*

Resonance Raman intensity analysis is an extremely powerful technique that can be useful to study the earliest (<50 fs) events occurring in photochemical and photophysical processes. It can provide detailed structural information about the CI dynamics and whether a CI occurs in or nearby the Franck–Condon region.[18–22] Our recent resonance Raman spectroscopic and CASSCF investigation of the Franck–Condon region structural dynamics and CIs of thiophene demonstrates clearly that the appearance of the intense non-totally symmetric vibrational fundamental modes and their large overtone and combination band progressions is an effective Raman marker for the existence of a CI in the Franck–Condon region.[20] In such special cases, the Herzberg–Teller vibronic-coupling mechanism lapses. The CI induces the breakdown of the Born–Oppenheimer approximation in its vicinity so that nonadiabatic transitions occur not only at the CI point but also in the extended area near the CI. Our resonance Raman spectroscopic and/or CASSCF investigations of the structural dynamics of benzamide[21] and tetra(4-aminophenyl) porphine[22] indicates that when a weak non-totally symmetric vibrational fundamental mode appears in the resonance Raman spectra, a CI point is likely demonstrated nearby than exactly in the Franck–Condon region. In this case, the PES in the Franck–Condon region of the bright excited state of interest, which dominates the resonance Raman scattering, is weakly perturbed by a dark coupling state that is nearby the Franck–Condon region, and Herzberg–Teller vibronic-coupling mechanism works reasonably well.

In this paper, we report the resonance Raman spectroscopy and CASSCF investigation of the vibronic couplings and the excited-state reaction dynamics of pyrazine in the $S_2(^1B_{2u}, {}^1\pi\pi^*)$ state to provide detailed information about the curve crossings between the bright S_2 state and the low-lying dark states. The wavelength dependence and/or solvent dependence of the curve crossings are examined. More than three states are discerned to exist somewhere away from the Franck–Condon region and couple with the bright $S_2(^1B_{2u})$ state through a likely Herzberg–Teller vibronic-coupling mechanism. An excited-state reaction mechanism of pyrazine is proposed on the basis of these experimental and computational results.

Experimental and computational methods

Resonance Raman experiments

The resonance Raman experimental methods and apparatus have been described previously,[23–26] so only a short description will be provided here. The harmonics of a nanosecond Nd : YAG laser and their hydrogen Raman shifted laser lines were employed to generate the 239.5 and 266 nm excitation wavelengths utilized in the resonance Raman experiments. Concentrations of approximately 0.025–0.045 M pyrazine (98% purity) in spectroscopic grade cyclohexane (99.5+ % purity) solvent were used to prepare sample solutions. The excitation laser beam used a ~100 μJ pulse energy loosely focused to a ~1.0 mm diameter spot size onto a flowing liquid stream of sample to excite the sample. Power-dependent experiments were performed using ~100 μJ pulse energy focused on a beam diameter of ~1.0 mm and ~260 μJ pulse energy focused on a beam diameter of ~0.5 mm, respectively. No power-dependent Raman peaks were found within the test conditions, and this indicated that there were no noticeable transients or photoproducts contributed to the resonance Raman spectra. A backscattering geometry was employed for collection of the Raman scattered light by reflective optics that imaged the light through a polarizer and entrance slit of a 0.5 m spectrograph, and the grating of the spectrograph dispersed the light onto a liquid nitrogen cooled charge-coupled device (CCD) mounted on the exit of the spectrograph. The CCD accumulated the Raman signal for about 100–120 s before being read out to an interfaced PC computer with 25–35 of these scans added together to obtain the resonance Raman spectrum. The Raman shifts of the resonance Raman spectra were calibrated with the known vibrational frequencies of the cyclohexane solvent Raman bands, and the solvent Raman bands were then subtracted from the resonance Raman spectra by utilizing an appropriately scaled solvent spectrum. Sections of the resonance Raman spectra were fit to a baseline plus a sum of Lorentzian bands to determine the integrated areas of the Raman bands of interest. The Fourier transform infrared (FT-IR) and FT-Raman spectra of pyrazine in the neat liquid were acquired, and the vibrational analysis were performed to help assign the Resonance Raman spectra of pyrazine. Depolarization ratio measurements were carried out with a Glan Prism polarizer that was placed in the scattered beam just before the entrance slit of the spectrograph,[27] and the polarization response of the spectrometer was referenced to the measurements of the cyclohexane bands that were employed as a standard. These three depolarized bands at 1347, 1226, and 1027 cm^{-1} gave ρ values of 0.75 ± 0.05, whereas the 802 cm^{-1} band was 0.13 ± 0.01. These values suggest that the measured values for pyrazine are affected neither by the polarization dependence of the grating efficiency nor by appreciable leak of the polarization analyzer.

Density functional theory and CASSCF computations

The stationary and transition structures of the ground and excited states of pyrazine and pyrimidine were optimized using the density functional theory (DFT) and CASSCF[28–30] methods. In this work, for the CASSCF calculations, the active space includes six electrons distributed over six valence orbitals, denoted as CASSCF (6,6) herein. They are four conjugated π orbitals (2π and 2π*) in the aromatic ring and two nonbonding orbitals on nitrogen atoms. The electronic transition energies were computed at the TDDFT/B3LYP/6-31G(d) and CASSCF (6,6)/6-31G(d) level. The nature of the minima and transition states (TSs) were verified by calculating the harmonic vibrational frequencies. All of the DFT and CASSCF calculations were performed with the Gaussian 03 program software suite.[31]

Time-dependent wave-packet calculations to model the resonance Raman intensities and absorption spectrum

The absorption spectrum and resonance Raman intensities were modeled by using Heller's time-dependent wave-packet approach.[27,32–34] The expression for the computed absorption spectrum is given by

$$\sigma_A(E_L) = \left(4\pi e E_L M_0^2/3n\hbar c\right) \int_{-\infty}^{\infty} G(\delta)\mathrm{d}\delta \mathrm{Re} \int_0^{\infty} \mathrm{d}t < 0|0(t) > \exp[i(E_L + \varepsilon_0)]t/\hbar] \times \exp[-\Gamma t/\hbar]$$

and the formula for the resonance Raman intensities is written as

$$\sigma_R(E_L) = (8\pi e^4 E_S^3 E_L M_0^4/9\hbar^6 c^4)\int_{-\infty}^{\infty} G(\delta)\mathrm{d}\delta \times |\int_0^{\infty} \mathrm{d}t < f|0(t)> \exp[i(E_L+\varepsilon_0)]t/\hbar] \times \exp[-\Gamma t/\hbar]|^2$$

where E_L is the incident photon energy, M_0 is the transition length evaluated at the equilibrium geometry, f is the final state for the Raman scattering, and n is the solvent index of refraction. The term $\exp[-\Gamma t/\hbar]$ is a homogeneous damping function that has contributions from the excited-state population decay and pure dephasing. $\delta = \hbar(\varpi_0 - \omega_0)$ is the shift from the central zero–zero frequency, ϖ_0, due to inhomogeneous broadening, and $G(\delta) = [1/\theta(2\pi)^{1/2}]\exp[-\delta^2/2\theta^2]$ is a normalized Gaussian distribution of site electronic energies. $|0(t)> = e^{-iHt/\hbar}|0>$, which is $|0>$ propagated on the excited-state surface for a time t and H, is the excited-state vibrational Hamiltonian.

Results and discussions

UV spectra and electronic transitions

The absorption spectra of pyrazine and the electronic structures of its low-lying excited states have been studied experimentally[35–38] and theoretically.[39] The vertical excitation energies of pyrazine were previously studied by Sugisaki *et al.* at CASSCF(10, 8)/cc-PVDZ and the multireference second-order perturbation theory MRMP2/cc-PVDZ level of theory computations.[39] In their work, the four singlet excited states were predicted to characterize the experimental observed absorption bands at 4.81, 6.51, and 7.67 (degenerate state) eV. The first singlet excited state, $S_1(^1B_{3u})$, is an n to π* transition, whereas the second singlet excited state, $S_2(^1B_{2u})$, exhibits a π to π* character.

Because some dark excited states may play an important role in coupling to the bright $S_2(^1B_{2u})$ state, we have carried out time-dependent DFT (TDDFT) calculations to determine the important dark excited states. The absorption cross sections of pyrazine in cyclohexane solution were also measured in order to simulate the absolute resonance Raman cross section and the experimental absorption cross section simultaneously and quantitatively by using Heller's time-dependent wave-packet approach to resonance Raman scattering. Figure 1 shows the UV spectrum of pyrazine in cyclohexane (solid line) and water (dotted line) with the excitation wavelengths indicated. There are two experimental absorption bands located in the region of 280–350 nm (A-band) and 220–280 nm (B-band), respectively. The molar extinction coefficients ε for B-band absorptions in water and cyclohexane are measured to be 4822 and 4427 l mol^{-1} cm^{-1}, respectively. Table 1 lists the TDDFT/B3LYP/6-31G(d) computed electronic transition energies, the molecular orbital numbers, and the oscillator strengths. Table 1 shows that among the electronic transitions in >200 nm UV spectral region, there are two calculated transition allowed electronic transitions at 307 nm (A-band) and 225 nm (B-band) with oscillator strengths $f = 0.0057$ and 0.0772, respectively. This is in good agreement with the experimental observed UV absorption bands at 315 nm ($f = 0.0096$) and 255 nm ($f = 0.0691$). Figure 2 shows the molecular orbitals associated with the electronic transitions of pyrazine. Orbitals 19, 20, 22, and 23 are π and π* orbitals, and they are respectively assigned as π_{H-2}, π_{H-1}, π_L, and π_{L+1}, whereas orbital 21 is respectively a nonbonding orbital. Thus, the main character of the A-band and B-band absorptions can be assigned respectively as the $n \rightarrow \pi_L$ and $\pi_{H-1} \rightarrow \pi_L$ transitions.

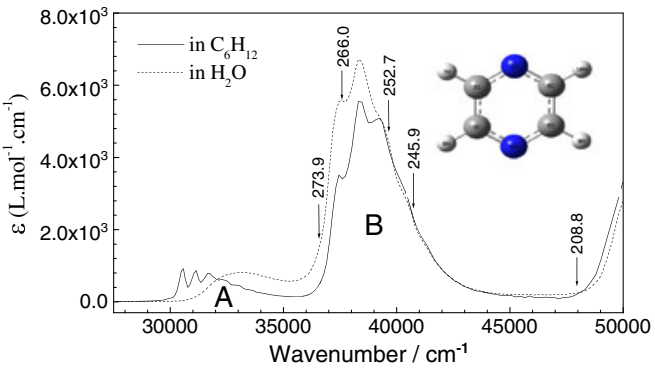

Figure 1. UV spectra of pyrazine in water and cyclohexane solvents with the excitation wavelengths for the resonance Raman experiments indicated above the spectrum.

The B-band absorption is clearly separated from the A-band in energy and is possibly a single, nondegenerate electronic state. It appears that the 245.9, 252.7, 266.0, and 273.9 nm excitation wavelengths used in the resonance Raman experiments are mostly on resonance with the B-band absorption of pyrazine. The depolarization ratio values for the intense or moderate intense Raman bands observed in the B-band resonance Raman in cyclohexane were measured, and the results were included in Table S1 in the Supporting Information. Most of measured depolarization ratio values are very close to $\rho = 1/3$ for pyrazine in cyclohexane solvent, which meets the selection rule that the depolarization ratio ρ should be 1/3 if the Raman intensity derives mostly from a single, nondegenerate electronic state in liquids at room temperature although some are significantly different from 1/3.

Vibrational assignments of resonance Raman spectra

The vibrational assignments of pyrazine were previously reported.[40] The FT-IR and FT-Raman spectra for pyrazine were measured (shown in Fig. S1 of the Supporting Information) and reassigned on the basis of results from the GAR2PED program[41] in this paper in order to better characterize the B-band resonance Raman vibrational modes of pyrazine, and these results are listed in Table 2.

The resonance Raman spectra of pyrazine resonant with the $S_1(^1B_{3u}, {}^1n\pi^*)$[42–45] and $S_2(^1B_{2u}, {}^1\pi\pi^*)$[46] states were previously measured. The B-band resonance Raman spectra taken by Suzuka *et al.* in the vapor phase at 266.0 nm excitation displayed bands that were attributed to the fundamentals, overtones, and combination bands of only two totally symmetric vibrations, namely the ring breathing mode ν_4 at 1015 cm^{-1} and the CNC deformation mode ν_5 at 596 cm^{-1}.[46] We have measured the B-band resonance Raman spectra of pyrazine in water and cyclohexane solvents in order to extract the underlying structural dynamics in the solution phase. Figures S2 and 3 show, respectively, the overall view and an enlarged view of the resonance Raman spectra of pyrazine in cyclohexane solvent. The spectra have been intensity corrected and the solvent subtracted. Most of the B-band resonance Raman spectra of pyrazine in cyclohexane solvent can be assigned to the fundamentals, overtones, and combination bands of about four Franck–Condon active modes as shown in Figs 3 and S2: the ring deformation mode ν_5 at 598 cm^{-1} and the ring breathing mode ν_4 at 1016 cm^{-1}, the C–H bend mode ν_3 at 1228 cm^{-1}, and the C–H bend + ring breathing/deformation mode ν_2 at 1572 cm^{-1}. The ring deformation mode ν_5, ring breathing mode ν_4, and their

Table 1. B3LYP/6-31G(d) computed electronic transition energy (ΔE) and oscillator strength (f) of pyrazine

States (D_{2h})		Orbitals	Characters	ΔE/nm					f	
				Calc.			Expt.		Calc.	Expt.
a	b					c		d		
$1\ ^1B_{3u}$ (x)	**S_1 (B_{3u})**	**21 → 22 (0.71)**	**$n_2 \rightarrow \pi_L^*$**	**307 nm**	**4.04 eV**		**315 nm**		**0.0057**	**0.0096**
$1\ ^1A_u$		21 → 23 (0.71)	$n_2 \rightarrow \pi_{L+1}^*$	264 nm	4.70 eV				0.0000	
$1\ ^1B_{2u}$ (y)	**S_2 (B_{2u})**	**18 → 23(−0.26)**	**$\pi_{H-1} \rightarrow \pi_{L+1}^*$**	**225 nm**	**5.52 eV**	**4.92 eV**	**255 nm**	**4.81 eV**	**0.0772**	**0.0691**
		20 → 22 (0.66)	**$\pi_H \rightarrow \pi_L^*$**							
$1\ ^1B_{2g}$		19 → 22 (0.70)	$n_1 \rightarrow \pi_L^*$	219 nm	5.67 eV				0.0000	
$1\ ^1B_{1g}$		19 → 23 (0.71)	$n_1 \rightarrow \pi_{L+1}^*$	193 nm	6.44 eV				0.0000	
$1\ ^1B_{1u}$ (z)	**S_3 (B_{1u})**	**18 → 22 (0.33)**	**$\pi_{H-1} \rightarrow \pi_L^*$**	**186 nm**	**6.67 eV**	**6.54 eV**		**6.51 eV**	**0.0614**	
		20 → 23 (0.62)	**$\pi_H \rightarrow \pi_{L+1}^*$**							
$2\ ^1A_u$		17 → 22 (0.71)	$\sigma \rightarrow \pi_L^*$	159 nm	7.81 eV				0.0000	
$2\ ^1B_{1u}$	**S_4 (B_{1u})**	**18 → 22 (0.61)**	**$\pi_{H-1} \rightarrow \pi_L^*$**	**156 nm**	**7.93 eV**	**7.20 eV**		**7.67 eV**	**0.3249**	
		20 → 23(-0.32)	**$\pi_H \rightarrow \pi_{L+1}^*$**							
$2\ ^1B_{2u}$	**S_5 (B_{2u})**	**18 → 23 (0.65)**	**$\pi_{H-1} \rightarrow \pi_{L+1}^*$**	**154 nm**	**8.03 eV**	**7.14 eV**		**7.67 eV**	**0.3076**	
		20 → 22 (0.25)	**$\pi_H \rightarrow \pi_L^*$**							

The boldface in Table 1 highlights the electronic transitions whose oscillator strengths have non-zero values.
[a]Values in parentheses are directions of the dipole transition moments.
[b]From Schneider and Domcke.[5]
[c]From Sugisaki *et al.*[39]
[d]From Weber and Reimers.[38]

Figure 2. Molecular orbitals associated with the electronic transitions of pyrazine.

overtones and combination bands dominate the B-band resonance Raman intensity, and this indicates that the short-time structural dynamics of pyrazine are mostly along the ring deformation and ring breathing reaction coordinates.

The intensity in the ν_2 band is likely influenced by some pre-resonance enhancement from the higher lying excited state because the ν_2 fundamental is one of the two predominate modes for the 208.8 nm resonance Raman spectrum and its intensity decreases as the excitation wavelengths increase, as depicted in Fig. S3. A weak non-totally symmetric vibrational mode (symmetric fundamental mode ν_{22} in the B_{2u} irreducible representation) at 1091 cm^{-1} appears in the 245.9 nm resonance Raman spectrum, whereas two weak non-totally symmetric fundamental modes, ν_{24} (B_{3u}) at 420 cm^{-1} and ν_6 (B_{1g}) at 913 cm^{-1}, appear in the 273.9 nm resonance Raman spectrum. This indicates that the $1\ ^1B_{2u}$ [or $S_2(^1B_{2u})$] excited state ($1\ ^1A_g \rightarrow 1\ ^1B_{2u}$ allowed transition) is coupled with some lower or upper excited states, as probed by the different laser excitation wavelengths.

Excited-state vibronic couplings

The Herzberg–Teller vibronic-coupling mechanism and the standard A-term mechanism are two rules that are frequently used in the vibrational assignments of some resonance Raman bands relative to non-totally symmetric fundamentals and/or their overtones. The standard A-term mechanism works if the vibrational frequency of a vibrational mode changes between electronically ground and excited states. In this case, the resonance Raman bands, which cannot be assigned as totally symmetric fundamentals and their overtones and combination bands, are assigned to the even overtones and/or combination bands of non-totally symmetric fundamentals. In contrast, Herzberg–Teller vibronic coupling[22,47] and Franck–Condon region CI mechanism[20,21] are used in the case when some Raman bands in the resonance Raman spectra can only be assigned as the non-totally symmetric fundamentals. Because no even overtones and/or combination bands of non-totally symmetric fundamentals are discerned in the 266.0, 252.7, and 245.9 nm resonance Raman spectra, the Herzberg–Teller rule is used to insight into the vibronic coupling between the different excited states.

According to the Herzberg–Teller mechanism,[47] if a two-state vibronic-coupling mechanism is applicable, the general rule for the transition polarizability tensor to be nonzero is that the product $\Psi_s Q_i \Psi_r$ belongs to a representation that contains the totally symmetric species (here, the subscript s and r denote two mutual coupled excited states, Q_i is a certain coupling vibrational mode). For vibronic coupling between $1\ ^1B_{2u}$ [$S_2(^1B_{2u})$] and $1\ ^1B_{3u}$ [$S_1(^1B_{3u})$], it comes out immediately that only those vibrational modes that have B_{1g} symmetry will possibly show up in the resonance Raman spectra because $B_{2u} \times B_{3u} = B_{1g}$, and this seems to be the case for the appearance of ν_6 (B_{1g}) at

Journal of RAMAN SPECTROSCOPY

Table 2. B3LYP/6-31G* calculated and experimental FT-Raman and FT-IR vibrational frequencies of pyrazine

Sym	Modes		Calc./cm^{-1}		Expt./cm^{-1}					Assignment, PED (%)
		[a]	[b]	[c]	FT-Raman	[a]	FT-IR	[a]	RR	
A_g	ν_1	ν_2	3197	3148		3053p				νC–H (100)
	ν_2	ν_{8a}	1633	1603	1581(s)	1579p	1576(w)		1572(s)	νRing (C–N) (44),δRing (18), δC–H (36)
	ν_3	$\boldsymbol{\nu_{9a}}$	1264	1239	1249(s)	1235p			1228(m)	δC–H (72)
	ν_4	$\boldsymbol{\nu_1}$	1046	1023	1014(vs)	1015p	1084(vs)		1016(vs)	νRing (88)
	ν_5	$\boldsymbol{\nu_{6a}}$	609	592	598(w)	601[f]	602(w)		598(vs)	δRing (61)
B_{1g}	ν_6	$\boldsymbol{\nu_{10a}}$	946	925		925[f]			913(w)[d]	γC–H (100)
B_{2g}	ν_7	ν_5	985	963		976[f]				γC–H (84),γRing (15)
	ν_8	ν_4	775	756		755[f]	777(m)			γRing (88)
B_{3g}	ν_9	ν_{7b}	3175	3126		3062dp				νC–H (100)
	ν_{10}	ν_{8b}	1594	1565	1522(m)	1522dp				νRing (C–N) (44),δRing (18)
	ν_{11}	ν_3	1388	1361	1359(w)	1353[f]				δC–H (88)
	ν_{12}	ν_{6b}	722	703	700(m)	698dp	694(w)		702(w)	δRing (62)
A_u	ν_{13}	ν_{17a}	993	971				977		γC2–H7 (92)
	ν_{14}	ν_{16a}	351	337						τRing (90)
B_{1u}	ν_{15}	ν_{13}	3176	3127				3015		νC–H (100)
	ν_{16}	ν_{19a}	1530	1501				1485		δC–H (76)
	ν_{17}	ν_{18a}	1172	1148			1163(vs)	1128		νC–N (52),δRing (45)
	ν_{18}	ν_{12}	1033	1011				1019		δRing (59)
B_{2u}	ν_{19}	ν_{20b}	3190	3141				3060		νC–H (100)
	ν_{20}	ν_{19b}	1457	1429				1411		δC–H (48),νRing (C C) (46)
	ν_{21}	ν_{14}	1244	1218				1339		νRing (98)
	ν_{22}	ν_{15}	1100	1077			1084(vs)	1065	1091(w)	δC–H (60),δRing (34)
B_{3u}	ν_{23}	ν_{11}	805	785			798(s)	790		γC–H (96)
	ν_{24}	ν_{16b}	435	420			469(s)	417	420(m)[e]	γRing (84)

The resonance Raman (RR) data are obtained from the 245.9 nm resonance Raman spectrum in cyclohexane solvent.
Sym: symmetry; vs: very strong; s: strong; m: middle; w: weak; ν: stretching, δ: in-plane bending, γ: out-of-plane bending; τ: torsion; Ring: pyrazine ring; PED, potential energy distribution; only contributions larger than 10% were given.
[a]From Billes *et al.*[40] (p: polarized; dp: depolarized).
[b]B3LYP/6-31G* calculated.
[c]Scaled = −9.66708 + 0.98762 × B3LYP/6-31G* calculated.
[d]From the 266.0 and 273.9 nm resonance Raman spectrum.
[e]From the 273.9 nm resonance Raman spectrum.
[f]From nonpolarized melt spectrum.

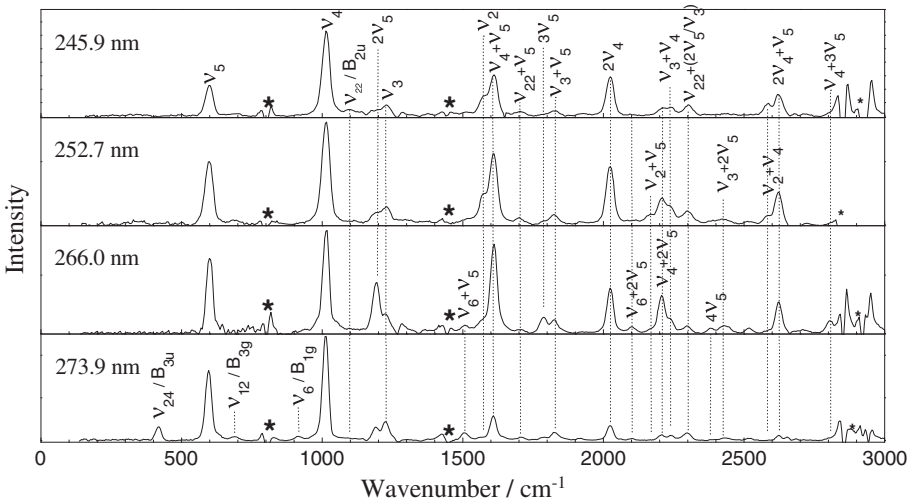

Figure 3. Enlarged view of resonance Raman spectra of pyrazine in cyclohexane solvent.

913 cm^{-1} in the 273.9 nm resonance Raman spectrum in Fig. 3. The intensity of the ν_6 (B_{1g}) fundamental or the overtone $2\nu_6$ in the 273.9 or 266.0 nm resonance Raman spectrum in Fig. 3 is weak. This indicates that the vibronic coupling in the Franck–Condon region between 1 $^1B_{2u}$ and 1 $^1B_{3u}$ states is weak or that the curve-crossing between 1 $^1B_{2u}$ and 1 $^1B_{3u}$ states takes place some distance away from the Franck–Condon region. Similarly, the appearance of the ν_{24} (B_{3u}) at 420 cm^{-1} in the 273.9 nm resonance Raman spectrum is due to vibronic coupling between 1 $^1B_{2u}$ [$S_2(^1B_{2u})$] and 1 $^1B_{1g}$ because $B_{2u} \times B_{1g} = B_{3u}$, whereas the appearance of the ν_{12} (B_{3g}) at 702 cm^{-1} in the 273.9 nm resonance Raman spectrum is due to vibronic coupling between 1 $^1B_{2u}$ [$S_2(^1B_{2u})$] and 1 $^1B_{1u}$ because $B_{2u} \times B_{1u} = B_{3g}$. In addition, the appearance of ν_{22} (B_{2u}) at 1091 cm^{-1} in the 245.9 nm resonance Raman spectrum in Fig. 3 is possibly due to the vibronic coupling between the higher lying excited states 1 $^1B_{1u}$ and 1 $^1B_{2g}$ because $B_{1u} \times B_{2g} = B_{2u}$, which supports an earlier suggestion that a vibronic coupling exists between the bright 1 $^1B_{2u}$ state and the (dark) 1 $^1B_{2g}$($n\pi^*$) state.[48,49]

Simulation of the B-band absorption and resonance Raman spectra

The theory of resonance Raman scattering from strongly vibronically coupled states (involving CIs) of polyatomic molecules has been developed earlier.[50] Most of the earlier reports on vibronic-coupling effects in resonance Raman spectra were within the framework of the Kramer–Heisenberg–Dirac formalism.[51–53] Time-dependent theory[32] was extended to curve-crossing problems[54–56] and has been used to a limited extent to study the dynamics on coupled states. Basically, the excited-state structural dynamics can be confined to a single adiabatic potential surface if the depolarization ratio values equal about 0.33 and when the inter-electronic state energy spacing are large or the CI is relatively far away from the Franck–Condon region.

We have chosen to model the relative intensities of the 245.9, 252.7, and 266.0 nm resonance Raman spectra and absorption spectra using the time-dependent wave-packet calculations and a simple model [27,32–34] because they are clearly mostly in resonance with the B-band absorption. Because the measured depolarization ratio value $\rho \approx 0.36$ is close to $\rho \approx 0.33$ for a single, nondegenerate electronic state, and the Raman intensity for coupling mode ν_6 (B_{1g}) at 913 cm^{-1} is very weak, it is expected that the vibronic coupling between the interested 1 $^1B_{2u}$ [or $S_2(B_{2u})$] state and 1 $^1B_{3u}$ [or $S_1(B_{3u})$] state is weak enough in the Franck–Condon region so that the interstate coupling by nuclear kinetic energy operator or transitions between the adiabatic electronic states in Franck–Condon region is small to negligible. Because it is unlikely that the dynamics can be followed to the minima of the excited-state PES, the normal mode displacements (Δ) may not be very useful to elucidate the initial Franck–Condon region dynamics. The absorption spectrum and resonance Raman intensity pattern are related to the excited-state potential surface in the Franck–Condon region, and the slope of the excited-state potential surface at the ground-state equilibrium geometry can help provide some insight into the Franck–Condon region PES. We have therefore estimated the excited-state slopes at the equilibrium ground-state geometry ($cm^{-1}/|\Delta|$) from the parameters used to fit the absorption and resonance Raman spectra, and these values are also listed in Table 3. Therefore, the extracted excited-state slope at the ground-state equilibrium geometry of the strongly Franck–Condon active vibrational modes of pyrazine in $S_2(^1B_{2u}, ^1\pi\pi^*)$ state may semi-quantitatively be used to estimate the degree of the structural reorganization required for pyrazine molecule to pass through the CI[$S_2(B_{2u})/S_1(B_{3u})$] point and to establish the correlation between the initial Franck–Condon dynamics revealed (by) time-dependent wave-packet calculations and the structural parameters of the CI[$S_2(B_{2u})/S_1(B_{3u})$] point predicted by CASSCF computations.

Table S2 presents the experimental and calculated absolute resonance Raman intensities. Table 3 presents the calculated parameters that best fit the data in the absorption spectrum and the intensities of the resonance Raman spectra. In order to simultaneously fit the absorption bandwidth and the pattern of the resonance Raman intensities, a large amount of electronic dephasing (the Γ parameter) was required to be included in the calculations, and this indicates that the population decay/electronic dephasing occurs substantially faster than just wave-packet motion away from the Franck–Condon region. The top of Fig. 4 shows a comparison of the calculated absorption spectrum (dotted line) with the experimental (solid line) absorption spectrum of pyrazine in cyclohexane solvent, whereas the bottom of Fig. 4 shows a comparison of the calculated resonance Raman cross sections (open bars) with the experimental Raman cross sections (solid bars) for the main features of the 245.9, 252.7, and 266.0 nm resonance Raman spectra of pyrazine in cyclohexane solvent. The results indicate that there is reasonably good agreement between the calculated and experimental absorption spectra while simultaneously providing a good fit to the absolute Raman intensities of the 245.9, 252.7, and 266.0 nm resonance Raman spectra for most overtones and combination bands. The simulations appear to overestimate the

Table 3. Parameters for the time-dependent wave-packet calculations and the resulting vibrational reorganizational energies for pyrazine in cyclohexane solution

Modes	Descriptions	Ground state Freq./cm^{-1}	Excited state Freq./cm^{-1}	$\|\Delta\|$	Estimated excited-state slope at ground-state equilibrium geometry ($cm^{-1}/\|\Delta\|$)
ν_5	δRing (61)	598	598	1.30	4.39×10^4
ν_4	νRing (88)	1016	1016	1.29	1.26×10^5
ν_3	δC–H (72)	1228	1228	0.78	1.11×10^5
ν_2	νRing (C–N) (44), δRing (18), δC–H (36)	1572	1572	0.23	5.37×10^4

Transition length $M = 0.482$ nm, $E_{00} = 37400$ cm^{-1}, $\Gamma = 320$ cm^{-1}.

Journal of RAMAN SPECTROSCOPY

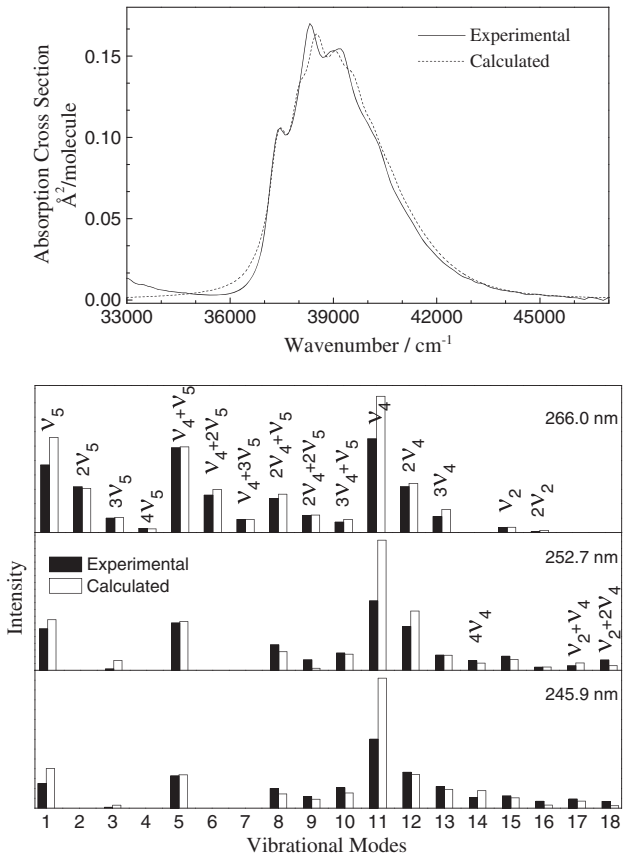

Figure 4. (Top panel) Comparison of the computed absorption spectrum (dotted line) with the experimental (solid line) absorption spectrum. (Bottom panel) Comparison of the computed resonance Raman cross sections (open bars) with the experimental Raman cross sections (solid bars) for the main Raman features of the 245.9, 252.7, and 266.0 nm resonance Raman spectra.

intensity in several of the fundamental resonance Raman bands (e.g. ν_4 and ν_5) in Fig. 4(b) and, this can be attributed to pre-resonance–resonance interference effects from higher lying excited states, which affect fundamental intensities much more than overtones and combination bands. The good agreement between the simulations and the experimental resonance Raman intensities for the $\nu_4+\nu_5$ combination band is consistent with this, and more weight was placed on fitting the combination bands and overtones when performing the simulations. Table 3 shows that the largest excited-state slopes at the ground-state equilibrium geometry occur with the ring breathing mode ν_4 ($1.26\times10^5\,cm^{-1}/|\Delta|$) and the C–H bend mode ν_3 ($1.11\times10^5\,cm^{-1}/|\Delta|$) and noticeable changes in the ring deformation mode ν_5 ($4.39\times10^4\,cm^{-1}/|\Delta|$) and the C–H bend + ring breathing/deformation mode ν_2 ($5.37\times10^4\,cm^{-1}\,|\Delta|$), respectively. The large excited-state slopes at the ground-state equilibrium geometry in ν_4 ($1.26\times10^5\,cm^{-1}/|\Delta|$), ν_5 ($4.39\times10^4\,cm^{-1}/|\Delta|$), and ν_3 ($1.11\times10^5\,cm^{-1}/|\Delta|$) correlate well with the large changes of the C–N/C=C bond lengths and CCN/CNC/CCH bond angles for CI point CI(S_2/S_1) as predicted by CASSCF method in following section.

Excited-state structures and reaction dynamics

As we focus on the photoisomerization process, we set our calculations on the singlet $^1\pi\pi^*$ excited states in which the reaction initiates. Two important conical intersections CI[$S_2(B_{2u})/S_1(B_{3u})$] and CI[S_1/S_0] of pyrazine are predicted at the CASSCF(6,6)/6-31G* level of theory, and their geometric structures are shown in Fig. 5. The N1–C2, N1–C6 and N4–C3, N4–C5 bond lengths for CI[$S_2(B_{2u})/S_1(B_{3u})$] are 0.1409 and 0.1403 nm respectively, which are much longer than the corresponding C–N bond lengths for S_0 (0.1331 nm). Similarly, the C2N1C6 and C3N4C5 bond angles for CI[$S_2(B_{2u})/S_1(B_{3u})$] are 125.2° and 127.6°, respectively, which are much larger than the corresponding CNC bond angles for S_0 (116.2°). The significant changes in the C–N bond length and CNC angle consist very well with the observed most intense resonance Raman bands of the ring deformation mode ν_5 at 598 cm^{-1} and ring breathing mode ν_4 at 1016 cm^{-1}. This suggests that the initial short-time structural dynamics of pyrazine in S_2 state is mostly involved in the coordinates of C–N bonds lengthening, C=C bonds shortening, and CNC bond angle enlarging. The large differences in the geometric parameters between CI[$S_2(B_{2u})/S_1(B_{3u})$] and S_0 indicate that CI[$S_2(B_{2u})/S_1(B_{3u})$] is significantly away from the Franck–Condon region. We thus conclude that the perturbation of S_2 PES in Franck–Condon region by the S_1 PES is very limited, and the modeling of the relative intensities of the B-band resonance Raman spectra and absorption spectra by using the time-dependent wave-packet calculations and a simple model is feasible. The geometric structures of CI[$S_2(B_{2u})/S_1(B_{3u})$] point is almost planarity, and this indicates that the Franck–Condon region structural dynamics is mostly along the in-plane vibrational reaction coordinates. This is in good agreement with the weak band intensities in ν_6 (B_{1g}) and its overtone $2\nu_6$ in the 273.9 and 266.0 nm resonance Raman spectra. It suggests that an out-of-plan deformation is required for the pyrazine molecule to evolve from CI[$S_2(B_{2u})/S_1(B_{3u})$] point to CI(S_1/S_0) point.

The TS is determined at both the CASSCF(6,6)/6-31G* and B3LYP/6-31G* level employing QST3 method. The TSs were verified by the intrisic reaction coordinate calculations. The corresponding structural parameters predicted at CASSCF(6,6)/6-31G* level are presented in Fig. 5. Figure 6 summarizes the photophysical processes and photoisomerization reaction between pyrazine and pyrimidine. As shown in Fig. 5, the TS structure is more analogous to the geometric structure of pyrimidine, whereas the CI(S_1/S_0) structure is more similar to the geometric structure of pyrazine. This suggests that the photoisomerization from pyrazine to pyrimidine can be achieved once the molecule passes over the TS and towards the S_0 PES of pyramidine, whereas the ground-state recovery of pyrazine can occur when the molecule passes over the CI(S_1/S_0) point and along the S_0 PES of pyrazine. Table 4 lists the CAS(6,6)/6-31G(d) calculated electronic excitation energies for the excited states S_1 and S_2 of pyrazine, the conical intersections CI[$S_2(B_{2u})/S_1(B_{3u})$] and CI(S_1/S_0) of pyrazine, and the transition barrier TS between ground-state pyrazine and pyrimidine. The CI[S_1/S_0] is a key intermediate point for the photoisomerization reaction to take place. It connects CI(S_2/S_1) and the TS. The CI[$S_2(B_{2u})/S_1(B_{3u})$] point is higher in energy (159 kcal mol^{-1}) than the CI[S_1/S_0] point (149 kcal mol^{-1}) by about 10 kcal mol^{-1}. The significant structural differences between the CI[S_1/S_0] and CI[$S_2(B_{2u})/S_1(B_{3u})$] points suggests that substantial geomerty reorganization takes place for pyrazine to evolve from $S_{2,FC}$ to the CI[$S_2(B_{2u})/S_1(B_{3u})$] point and then to the CI[S_1/S_0] point. Pyrazine in the CI[S_1/S_0] point can either evolve into S_0 (pyrazine) or TS. Because CI[S_1/S_0] is higher in energy than TS by about 37 kcal mol^{-1}, the shuttling motion of the N atom (from the CI[S_1/S_0] point to the TS point) is favorable energetically. Once the molecule evolves into the TS region, pyrimidine will be formed.

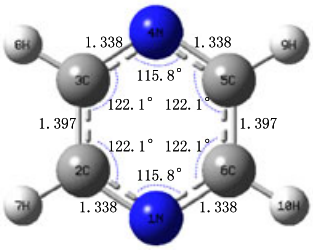

S_0(Pyrazine)(B3LYP)

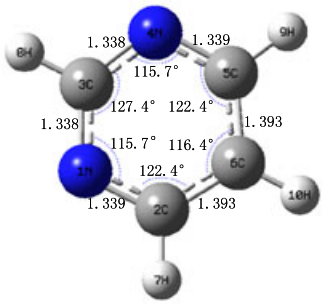

S_0(Pyrimidine)(B3LYP)

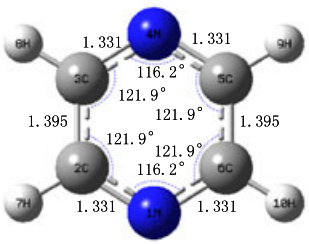

S_0(Pyrazine)(CAS)

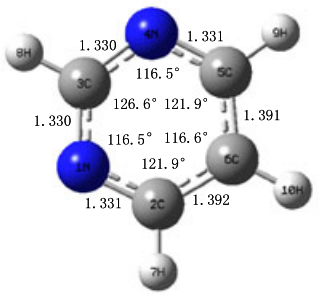

S_0(Pyrimidine)(CAS)

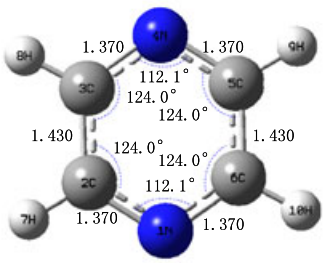

S_1(Pyrazine) (CAS)

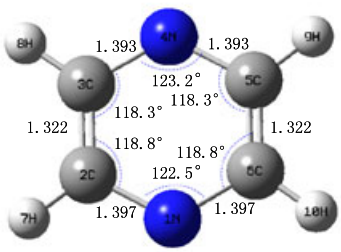

S_2(Pyrazine) (CAS)

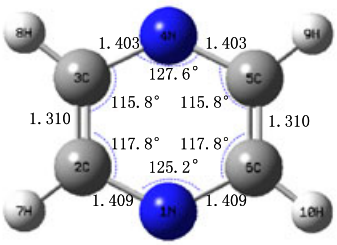

CI[$S_2(B_{2u})/S_1(B_{3u})$] (CAS)

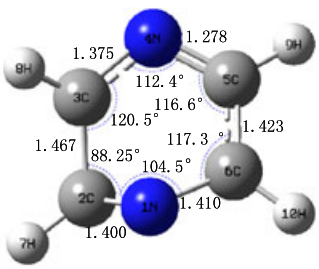

CI(S_1/S_0)(CAS)

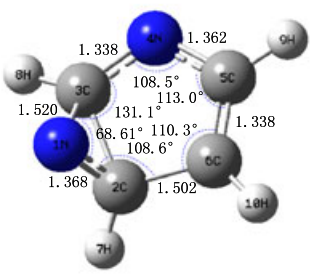

TS (CAS)

Figure 5. The CASSCF(6,6)/6-31G* predicted geometry structures for the conical intersections CI[$S_2(1\ ^1B_{2u})/S_1(1\ ^1B_{3u})$] and CI[$S_1(B_{2u})/S_0$] of pyrazine and for the transition states (TSs) between pyrazine and pyrimidine.

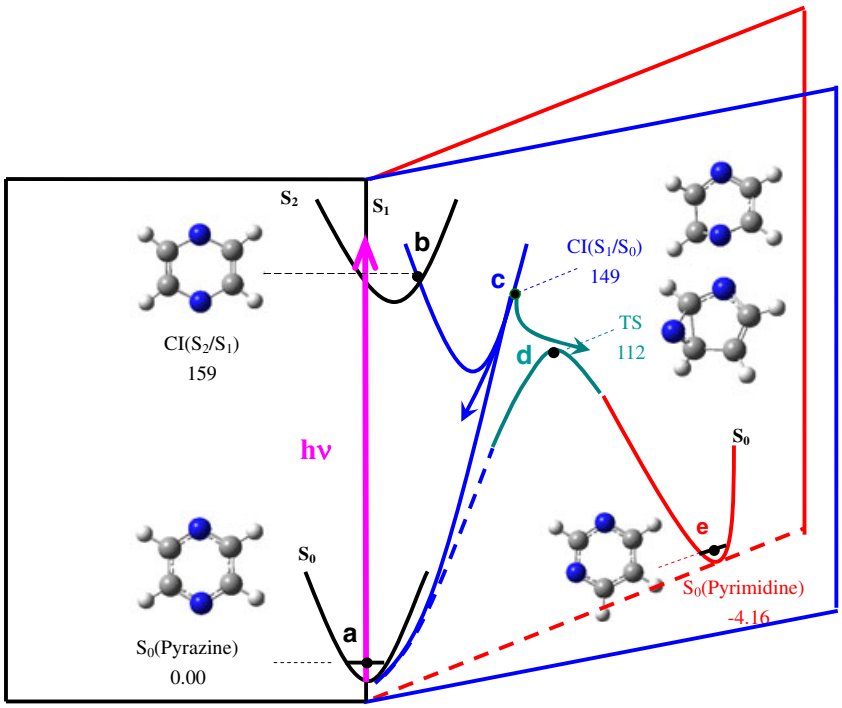

Figure 6. Potential energy surface diagram for photoinduced isomerization reactions between pyrazine and pyrimidine. The minimum energy for points a–e are calculated by the CASSCF(6,6)/6-31G* level of theory. Values are in kcal/mol.

Table 4. CAS(6,6)/6-31G(d) calculated electronic excitation energies for the excited states S_1 and S_2 of pyrazine, the conical intersections CI[$S_2(B_{2u})$/$S_1(B_{3u})$] and CI(S_1/S_0) of pyrazine, and the transition barrier TS between ground-state pyrazine and pyrimidine

Geometry	Energy/arb. units	Transition energy/kcal mol^{-1}
Pyrazine S_0	−262.7652744	0
Pyrimidine S_0	−262.7719041	−4.16 (−4.07)[a]
Pyrazine S_1	−262.5880470	111
Pyrazine S_2	−262.5303644	147
Pyrazine CI[$S_2(B_{2u})/S_1(B_{3u})$]	−262.5122198	159
Pyrazine CI(S_1/S_0)	−262.5272123	149
TS	−262.5862235	112

[a]Value in parentheses is calculated from B3LYP/6-31G(d) level of theory.

Conclusion

The photophysics and photochemistry of pyrazine ($C_4H_4N_2$, D_{2h}) after excitation to the S_2 (1 $^1B_{2u}$, $^1\pi\pi^*$) electronic state were studied by using the resonance Raman spectroscopy and CASSCF method calculations. The B-band absorption and resonance Raman spectra were simulated by using time-dependent wave-packet calculations, and these results indicate that the largest changes in the excited-state slopes in the Franck–Condon region occur with the ring breathing mode ν_4, the ring deformation ν_5, and the C–H bend mode ν_3. Three excited states that have 1 $^1B_{3u}$, 1 $^1B_{1g}$, and 1 $^1B_{2g}$ irreducible representations were found to couple with the S_2 (1 $^1B_{2u}$) state. Two CI points CI[$S_2(B_{2u})/S_1(B_{3u})$] and CI[S_1/S_0] and one TS of the ground-state isomerization reaction between pyrazine and pyrimidine are respectively predicted at the CASSCF(6,6)/6-31G(d) and/or B3LYP/6-31G(d) level of calculations. The CI[S_1/S_0] is a key intermediate point that connects the CI(S_2/S_1) and the TS. Once the molecule evolves into the TS region, pyrimidine will be formed. The photoisomerization reaction mechanism from pyrazine to pyrimidine is proposed as follows:

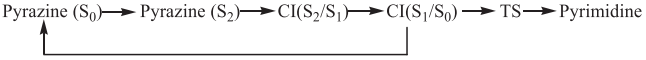

Acknowledgements

This work was supported by grants from NNSFC (no. 21033002) and the National Basic Research Program of China (2007CB815203).

Supporting information

Supporting information may be found in the online version of this article.

References

[1] W. Domcke, D. R. Yarkony, H. Koppel. *Conical Intersections: Advanced Series in Physical Chemistry*, vol. *15*, World Scientific, Singapore, **2004**.
[2] J. S. Lim, S. K. Kim, *Nat. Chem.* **2010**, *2*, 627.
[3] T. Tahara, H. Hamaguchi, *Rev. Sci. Instrum.* **1994**, *65*, 3332.
[4] C. E. Crespo-Hernández, B. Cohen, P. M. Hare, B. Kohler, *Chem. Rev.* **2004**, *104*, 1977.
[5] R. Schneider, W. Domcke, *Chem. Phys. Lett.* **1988**, *150*, 235.
[6] L. Seidner, G. Stock, A. L. Sobolewski, W. Domcke, *J. Chem. Phys.* **1992**, *96*, 5298.
[7] C. Woywod, W. Domcke, A. L. Sobolewski, H.-J. Werner, *J. Chem. Phys.* **1994**, *100*, 1400.
[8] A. Stolow, A. E. Bragg, D. M. Neumark, *Chem. Rev. (Washington, D.C.)* **2004**, *104*, 1719.
[9] I. V. Hertel, W. Radloff, *Rep. Prog. Phys.* **2006**, *69*, 1897.
[10] Y.-I. Suzuki, T. Fuji, T. Horio, T. Suzuki, *J. Chem. Phys.* **2010**, *132*, 174302.
[11] F. Lahmani, N. Ivanoff, M. Magat, *C. R. Acad. Sci, Paris* **1966**, *263*, 1005.
[12] F. Lahmani, N. Ivanoff, *Tetrahedron Lett.* **1967**, *8*, 3913.
[13] F. Lahmani, N. Ivanoff, *J. Phys. Chem.* **1972**, *76*, 2245.
[14] A. Lablache-Combier, in *Photochemistry of Heterocyclic Compounds* (Ed.: O. Buchardt), Wiley, New York, **1976**, Chapter 4, and references there in.
[15] El-Sayed, M. A. *J. Chem. Phys.* **1962**, *36*, 573.
[16] El-Sayed M. A. *J. Chem. Phys.* **1963**, *38*, 2834.
[17] M.-D. Su, *J. Phys. Chem. A* **2006**, *110*, 9420.
[18] P. J. Reid, M. K. Lawless, S. D. Wickham, R. A. Mathies, *J. Phys. Chem.* **1994**, *98*, 5597.
[19] A. B. Myers, *Acc. Chem. Res.* **1997**, *30*, 519.
[20] X. F. Wu, X. M. Zheng, H. G. Wang, Y. Y. Zhao, X. G. Guan, D. L. Phillips, X. B. Chen, W. H. Fang, *J. Chem. Phys.* **2010**, *133*, 134507.
[21] K. M. Pei, Y. F. Ma, X. M. Zheng, *J. Chem. Phys.* **2008**, *128*, 224310.
[22] H. G. Wang, J. Xu, J.M. Wan, Y. Y. Zhao, X. M. Zheng, *J. Phys. Chem. B* **2010**, *114*, 3623.
[23] W. M. Kwok, D. L. Phillips, *J. Chem. Phys.* **1996**, *104*, 2529.
[24] X. M. Zheng, Y. L. Li, D. L. Phillips, *J. Phys. Chem. A* **2004**, *108*, 8032.
[25] X. M. Zhu, S. Q. Zhang, X. Zheng, D. L. Phillips, *J. Phys. Chem. A* **2005**, *109*, 3086.
[26] K. F. Weng, Y. Shi, X. M. Zheng, D. L. Phillips, *J. Phys. Chem. A* **2006**, *110*, 851.
[27] A. B. Myers, in *Laser Techniques in Chemistry* (Eds: A. B. Myers, T. R. Rizzo), Wiley, New York, **1995**, pp. 23, 325.
[28] A. Becke, *J. Chem. Phys.* **1986**, *84*, 4524.
[29] C. Lee, W. Yang, R. G. Parr, *Phys. Rev. B.* **1988**, *37*, 785.
[30] D. Hegarty, M. A. Robb, *Mol. Phys.* **1979**, *38*, 1795.
[31] M. J. Frisch, G. W. Trucks, H. B. Schlegel, G. E. Scuseria, M. A. Robb, J. R. Cheeseman, J. A. Montgomery Jr, T. Vreven, K. N. Kudin, J. C. Burant, J. M. Millam, S. S. Iyengar, J. Tomasi, V. Barone, B. Mennucci, M. Cossi, G. Scalmani, N. Rega, G. A. Petersson, H. Nakatsuji, M. Hada, M. Ehara, K. Toyota, R. Fukuda, J. Hasegawa, M. Ishida, T. Nakajima, Y. Honda, O. Kitao, H. Nakai, M. Klene, X. Li, J. E. Knox, H. P. Hratchian, J. B. Cross, C. Adamo, J. Jaramillo, R. Gomperts, R. E. Stratmann, O. Yazyev, A. J. Austin, R. Cammi, C. Pomelli, J. W. Ochterski, P. Y. Ayala, K. Morokuma, G. A. Voth, P. Salvador, J. J. Dannenberg, V. G. Zakrzewski, S. Dapprich, A. D. Daniels, M. C. Strain, O. Farkas, D. K. Malick, A. D. Rabuck, K. Raghavachari, J. B. Foresman, J. V. Ortiz, Q. Cui, A. G. Baboul, S. Clifford, J. Cioslowski, B. B. Stefanov, G. Liu, A. Liashenko, P. Piskorz, I. Komaromi, R. L. Martin, D. J. Fox, T. Keith, M. A. Al-Laham, C. Y. Peng, A. Nanayakkara, M. Challacombe, P. M. W. Gill, B. Johnson, W. Chen, M. W. Wong, C. Gonzalez, Pople J. A., Gaussian 03, Revision B.05, Gaussian, Inc., Pittsburgh, PA, **2003**.
[32] S. Y. Lee, E. J. Heller, *J. Chem. Phys.* **1979**, *71*, 4777.
[33] E. J. Heller, R. Sundberg, D. Tannor, *J. Phys. Chem.* **1982**, *86*, 1822.
[34] A.B. Myers. R. A. Mathies, in *Biological Applications of Raman Spectroscopy*, vol. 2, (Ed.: T. G. Spiro), Wiley, New York, **1987**, Chapter 1.
[35] B. I. Yamazaki, T. Murao, T. Yamanaka, K. Yoshihara, *Faraday Discuss. Chem. Soc.* **1983**, *75*, 395.
[36] K. K. I. Innes, G. Ross, W. R. Moonaw, *Mol. Spectrosc.* **1988**, *132*, 492.
[37] D. B. McDonald, S. A. Rice, *J. Chem. Phys.* **1981**, *74*, 4893.
[38] P. Weber, J. R. Reimers, *J. Phys. Chem. A* **1999**, *103*, 9821.
[39] K. Sugisaki, K. Toyota, K. Sato, D. Shiomi, M. Kitagawa, T. Takui, *Chem. Phys. Lett.* **2009**, *477*, 369.
[40] F. Billes, H. Mikosch, S. Holly, *J. Mol. Structure (Theochem)* **1998**, *423*, 225.
[41] J. M. L. Martin, C. Van Alsenoy, GAR2PED, University of Antwerp, **1995**.
[42] I. Suzuka, N. Yikami, Y. Udagawa, K. Kaya, M. Ito, *J. Chem. Phys.* **1972**, *57*, 4500.
[43] M. Ito, I. Suzuka, Y. Udagawa, N. Mikami, K. Kaya, *Chem. Phys. Lett.* **1972**, *16*, 211.
[44] A. H. Kalanter, E. S. Franzosa, K.K. Innes, *Chem. Phys. Lett.* **1972**, *17*, 335.
[45] H. K. Hong, C.-W. Jacobsen, *J. Chem. Phys.* **1978**, *68*, 1170.
[46] I. Suzuka, Y. Udagawa, M. Ito, *Chem. Phys. Lett.* **1979**, *64*, 333.
[47] D. J. Swanton, G. B. Bacskay, N. S. Hush, *Chem. Phys.* **1984**, *83*, 69.
[48] W.R. Wadt, W.A. Goddard III, T. H. Dunning Jr, *J. Chem. Phys.* **1976**, *65*, 438.
[49] K. Jug, G. Hahn, *J. Comput. Chem.* **1983**, *4*, 410.
[50] G. Stock, W. Domcke, *J. Chem. Phys.* **1990**, *93*, 5496.
[51] W. H. Henneker, W. Siebrand, M. Z. Zgierski, *Chem. Phys. Lett.* **1976**, *43*, 11.
[52] W. H. Henneker, A. P. Penner, W. Siebrand, M. Z. Zgierski, *Chem. Phys. Lett.* **1977**, *48*, 197.
[53] M. Z. Zgierski, M. Pawlikowski, *Chem. Phys. Lett.* **1979**, *63*, 221.
[54] R. Heather, H. Metiu, *J. Chem. Phys.* **1989**, *90*, 6903.
[55] R. D. Coalson, J. L. Kinsey, *J. Chem. Phys.* **1986**, *85*, 4322.
[56] P. D. Chowdary, S. Umapathy, *J. Raman Spectrosc.* **2010**, *41*, 310.